

Experimental Study of Hydroformed Al6061T4 Elliptical Tube Samples under Different Internal Pressures

Md. Meraz, Santosh Kumar, Ravi Prakash Singh

Department of Mechanical Engineering, Indian Institute of Technology (Banaras Hindu University) Varanasi, India

Correspondence Author: mdm.rs.mec16@itbhu.ac.in

Received September 6, 2022; Revised October 7, 2022; Accepted November 9, 2022

Abstract

In order to achieve crack free elliptical shape under controlled conditions, an experimental set-up was designed and fabricated. This setup consists of three hydraulic cylinders, an intensifier, a hydraulic power pack, storage tanks, forming die, and all parts are controlled by a Programmable Logic Controller (PLC) system. The elliptical samples can be achieved through proper control of internal pressure and axial force with proper sealing. Experimental work has been carried out with different magnitudes of internal pressure and constrained conditions of axial force. Initially die of elliptical shape has been designed and modeled in Abaqus to successfully achieve the particular shape of the Al6061T4 tube under different internal pressure. The fabricated tube hydroforming machine set-up is highly effective for forming 0.5 mm-2 mm thick Al6061T4 alloy tube samples. The Experimental test has been carried out at 12.7 mm outer diameter, 175 mm length and 0.5 mm thick Al6061T4 samples. Bulge height parameters measured at different points of regular distance gap on the axial direction of the tube length and corner radius found at different pressures range of the samples are plotted under different internal pressures. Samples having an 18.7 mm major elliptical bulge were achieved during the experiment. The experimental data was validated by simulation results.

Keywords: Internal Pressure, Bulge height, Corner radius, Elliptical bulge, Tube Hydroforming.

1. INTRODUCTION

The main aim of industries and researchers is to reduce structural weight along with less energy intake during the competitive rise and rapid growth in the field of automobile and aviation industries [1]. Hollow structural parts manufactured through hydroforming technology are highly efficient and environmentally friendly, which are capable of not only reducing the body weight but, simultaneously it is reducing the time, energy, and materials. With these benefits, hydroforming has emerged as the main source for manufacturing lightweight structures. Even dissimilar thickness metals

can be formed using this technique [2]. Intricate shapes and designs are massively used in the automobile and aerospace sectors which also draws attention to such techniques [3]. The above papers not only summarize the technical examination of the hydroforming process but also prove that such techniques are more beneficial for the mass production of hollow and lightweight aluminium and magnesium alloys used in automobiles and aviation industries and allow the researchers to focus on various methods such as materials selections, die and tooling design, die corner radius, axial feeding force, internal pressure, coefficient of friction, etc. It is important to look technically at the detailed study of the process available for tube hydroforming and what is the best possible option suited for the experimental specification from the given available options [4]. It was found that the tube can be hydroformed either by only the action of internal pressure inside the sample, the tube is subjected to high pressure and end sealing helps in the gradual increase of internal pressure. This increasing internal pressure gradually bulges out the samples as per the cavity dimensions present in the die or with the simultaneous combination of axial force and pressurized fluid internally in the tube sample, the tube is pushed with the help of internally generated liquid pressure to the required die slot and forms final components. In order to design and decide the capacity of the final fabricated tube hydroforming machine setup for given elliptical aluminium 6061T4 sample size, it is important to analyze numerically through simulation the material behavior at different parameters such as internal pressure effects on material failure including wall thinning, buckling, wrinkling and folding etc. Improving bulging and minimizing thinning is also carried out in order to get better results [5]. An Artificial Neural Network (ANN) approach also plays an important role while predicting parameters used in Tube Hydroforming process [6]. The loading path followed during tube hydroforming friction factors and forming limit diagram are important parameters for analyzing material failure.

2. RELATED WORK

A two-dimensional hydroforming investigation of Al6260T4 tubes was presented by Korkolis and Kyriakides. The main issue encountered during the investigation was localized wall thinning at the center because of frictional impact which results in bursts and difficulties in corner filling. Nowadays, many researchers discuss enhancing material forming quality. Hashemi et al. [7] explained about forming limit diagram using an extended strain with the inverse finite element method (IFEM) to generate a rapid calculation for tube length, fluid pressure and axial feeding in tube hydroforming. So IFEM may be turned into a fast simulation method to predict the tube hydroforming parameters. Tube buckling, wrinkling and folding limit also affect the loading path before reaching the targeted internal pressure. Hill's yield, as well as Hosford's yield criterion, are used in the wrinkling limit. However, Hosford's yield criterion is a better tool compared to Hill's yield criterion, for the

prediction of the bursting limit. Punch and die design were simulated for tube hydroforming techniques by Gracious Ngaile and James Lawrie [9]. The forming process and Formability of thin-walled tubes under hydraulic bulging, hydroforming with radial crushing and liquid impact forming was used by Xiangwen Fan et. al. [10]. FEA analysis carried out using LS DYNA to study the thickness distribution using beneficial wrinkles and preform shape [11]. Yuan and Wang [12] constructed a setup that is capable of explaining the surface wrinkling features of less thick wall shells subjected to both actions of internal and exterior pressures simultaneously in a two-sided tube hydroforming setup, which assured that there is no involvement of external pressure on tube wrinkling. The stress-strain states and yield locus during hydroforming are comprehensively illustrated by Shijian Yuan. The stress locus of tube hydroforming is presented. Finally, the stress-state of corner zone and the splitting mechanism are discussed. [13]. Double-sided tube hydroforming-bulging was proposed by Xiao-Lei Cui to provide a beneficial three-dimensional stress state in the deformation zone of the tube, so as to delay the occurrence of bursting on the tube [16]. All the above proposed methods help in improving experimental design and setup of die and tooling. It not only reduces friction factor by applying proper die corner radius and lubrication but also helps in complete filling of material and protects the samples from failure. The above literature studies reveal that increased internal pressure is different from the thickness of the pipes, which reduces the uniformity of the part at the corners but improves bulge height. The quality of hydroforming parts can be related to the uniform wall thickness and thinning which causes bursting and failure of samples. Also, Finite element methods are an important tool for numerically predicting the effects of the initial diameter of tube and wall thickness on shape conformation, optimal internal pressure, and axial force. The THF of circular cross-section steel tubes was investigated using FEM modeling. Internal pressure, loading path, axial feed, and friction coefficients of 0.05 were used to compute the friction coefficients [18]. Tube hydroforming (THF) was used to evaluate experimentally and numerically the impact of internal pressure and axial compressive displacement on the formability of small-diameter magnesium alloy taper tubes [19]. These articles examined sample buckling and the deformation behavior of various factors. The impact of the loading path and punch shape on the thickness distribution and deformation behavior of aluminium alloy tube samples was examined [20]. Hydroforming uses have increased gradually over the last couple of decades and cover almost every field including automotive and aircraft industries as well as in the manufacturing of components for sanitary use. Automotive applications can be seen in exhaust parts, camshafts, radiator frames, front and rear axles, engine cradles, crankshafts, seat frames, body parts and space frames. Some well-known applications are BMW-rear axle of 500 series, Mercedes Benz exhaust manifolds, Buick Park Avenue-roof rail inner and engine cradle, Corvette-lower rails, roof bow and instrument panel beam [15]. Defect

analysis in tube hydroforming is another parameter. The optimal loading path to prevent defects including insufficient bulging and wrinkles were analytically determined and verified through experiments by Han S. et. al. [21]. Wrinkling defects in tube hydroforming reduce using preheating by Kong TF et. al. [22]. Numerical and analytical solutions are compared for the internal pressure required to bulge and burst the tube by Reddy PV et. al. [23]. Colpani A et. al. study focuses on the characterization and optimization of the THF process for stainless steel T-joint parts produced in two sizes: small and large [24]. Zhu H et. al. developed a theoretical analysis model for tube hydro-bulging tests first. And then the stress paths and strain paths during bulging with fixed-ends and free-ends are analyzed through the theoretical model and finite element simulations [25].

3. ORIGINALITY

In order to determine the variation of corner radius and bulge height for rectangular and circular tubes, various research and studies on increasing fluid pressure during the tube hydroforming process are conducted. Still, there is a research gap for elliptical tubes with complex shape samples. Therefore, we are utilizing elliptical dies to understand the variation of tube bulge height and corner radius along the bends and the bulge region of the elliptical tube at different pressure ranges.

In this paper, the experiments on bulge height and corner radius of an Al6061T4 hydroformed elliptical tube have been investigated using a self-fabricated experimental tube hydroforming test system. Simulation studies of the tube hydroforming process have also been conducted using nonlinear finite element software. Since ideal boundary conditions were adopted for the simulation so definitely there is a deviation between experimental and simulated obtained data. The deviation of simulation bulge height and corner radius data with experimental ones was plotted at different internal pressures.

4. SYSTEM DESIGN

4.1. 3D CAD model and fabricated Setup

A tube hydroforming experimental system has been developed to investigate the elliptical cross-sectional bulge height distribution and corner radius along the tube length. The 3D model and fabricated system are shown in fig.1 (a) and (b) respectively. Table 1 describes the components used in the hydroforming setup. The experimental system consists Programmable Logic controllers (PLCs), a power pack containing pump driving three cylinders, two pressure gauges, metallic hose pipe, sealing ends, storage tanks for water and oil, a die with elliptical cavity and pressure intensifier. During the hydroforming process, the upper vertical cylinder guarantees that the upper and lower dies are completely closed. Pressure intensifier provides required pressure for the tube samples with water as medium. The gauge pressure range is from 0 to 100 MPa. The gauge is connected between intensifier and

die cavity to measure pressure during the process. When the button is pressed then upper die is closed tightly with the lower die during the forming process. The maximum holding force of the upper cylinder is 1000 kN. The pressure inside the tube increases gradually and reaches the required level where the tube starts bulging. Timer set on the PLC as 5 seconds which is enough for intensifier to generate required pressure for bulging. For the next 5 seconds, PLC releases the pressure by reversing the intensifier stroke. Once tube got bulge, PLC commanded the pairs of die to unlock followed by releasing the pressure by opening the seals at tube ends to complete the process.



Figure 1(a)



Figure 1(b)

Figure 1(a). 3D model; **(b).** Fabricated elliptical tube hydroforming setup.

Table 1. Description of various components as designated in fig. 1(a).

Designated No	Description
1	Upper vertical cylinder
2	Right side horizontal cylinder
3	Left side horizontal cylinder
4	Die arrangement for bulge tube hydroforming
5	Hydraulic pressure intensifier (boost pressure from atmospheric to 1000 bar)
6	Hydraulic power pack 200 L oil storage capacity (control the motion of the vertical and horizontal cylinder through hose pipe connections)
7	Water storage tank (100 L)
8	Hose pipe connections on the power pack
9	Power pack motor (5 kW)
10	Water storage tank motor to supply water from tank to intensifier
11	Supporting structure
12	Split check valve

4.2. Die Design and Formed tube sample

The die is made of SLD10 die steel having a hardness between 62-64 HRC. Die cavity component is designed and fabricated with the required elliptical shape as shown in fig. 2 (a) and (b) respectively.

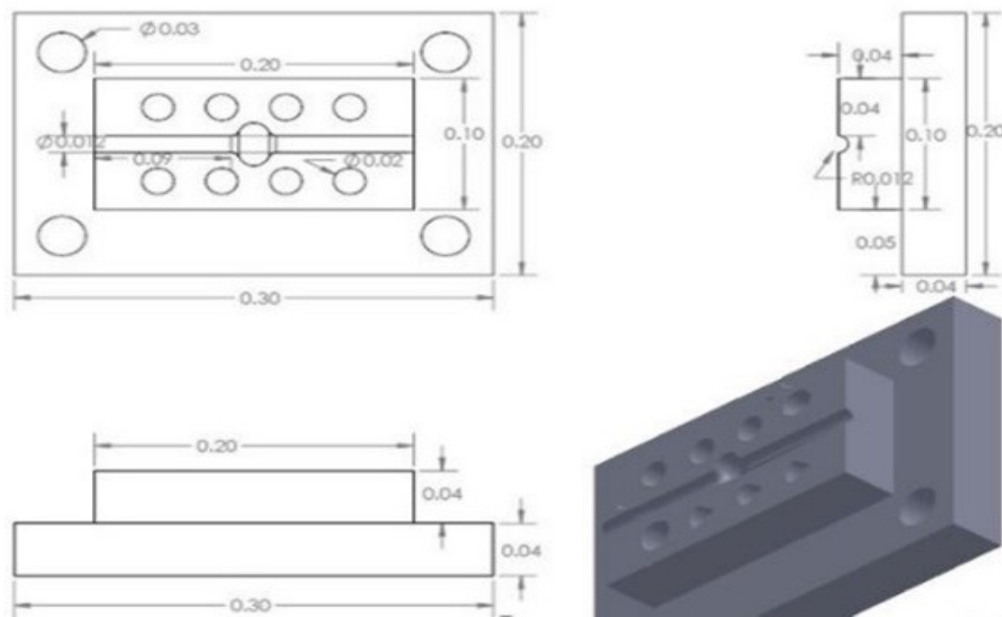


Figure 2(a)



Figure 2(b)

Figure 2(a). Sketch of tube hydroforming half die (dimensions are in meter); **(b).** Fabricated tube hydroforming half die.

The length of the slot containing the die is 200 mm. A sealing plug of 15 mm is inserted on both ends to seal the die cavity. The sample tube length is 175 mm (shown in fig. 3 (a) and (b)). The length, height, fillet radius and width of the forming zone are 30 mm, 2.5 mm, 5 mm and 18.7 mm respectively.

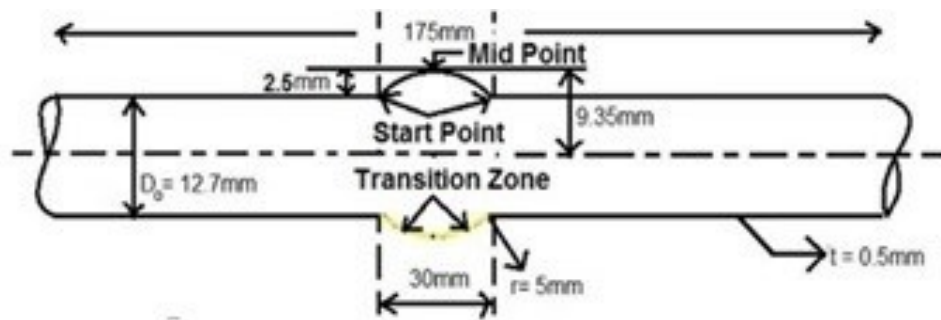


Figure 3(a)



Figure 3(b)

Figure 3(a). Layout of formed tube sample; (b). Formed tube sample.

5. EXPERIMENT AND ANALYSIS

5.1. Finite element analysis

To perform challenging research with a directional valuable solution by giving clear insight into complex systems of hydroforming and to study its parameter which affects the sample wall thickness during the forming process, finite element software having nonlinear property was used. Finite element analysis of elliptical tube hydroforming was developed in Abaqus software with some experimental conditions. The analysis includes a die which is rigid, deformable tube with the same condition of internal pressure and constrained axial force. Half die-tube wall interface profile was drawn and meshed instead of a whole die drawing to reduce the computational time. Only the half-elemental surface of the required rigid die was defined. The finite element model and specification of the tube sample are shown in fig. 4 (a) and (b) and table 2 respectively.

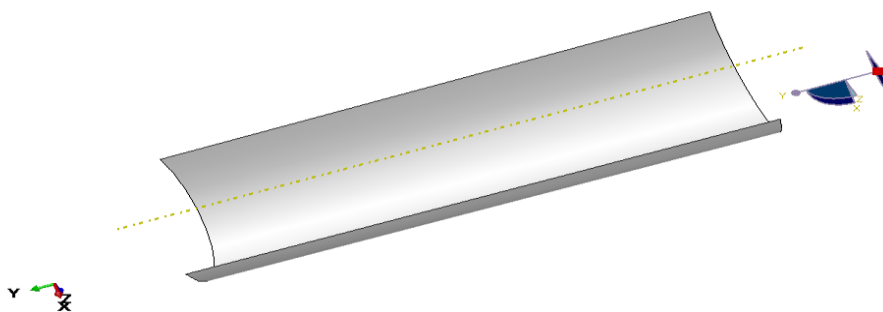


Figure 4(a)

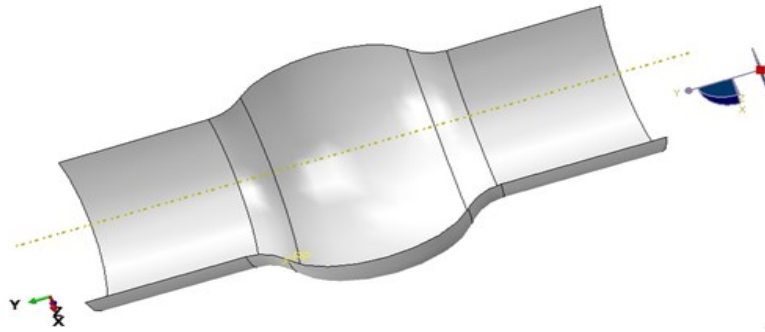


Figure 4(b)
Figure 4(a). CAD model of tube wall interface; **(b).** Die wall interface drawn in Abaqus.

Table 2. Specification of tube sample

S No.	Dimension of Tube	Length (mm)
1	Length (L)	175±0.5mm
2	Internal diameter (Di)	11.7±0.1mm
3	Outer diameter (Do)	12.7±0.1mm
4	Thickness (to)	0.5 ^{0.05} mm

The material properties of the Al tube have been chosen from the standard data. During simulation, the coefficient of friction for an ideal condition is taken as 0.1. The pressure vs time loading graph is shown in fig.5.

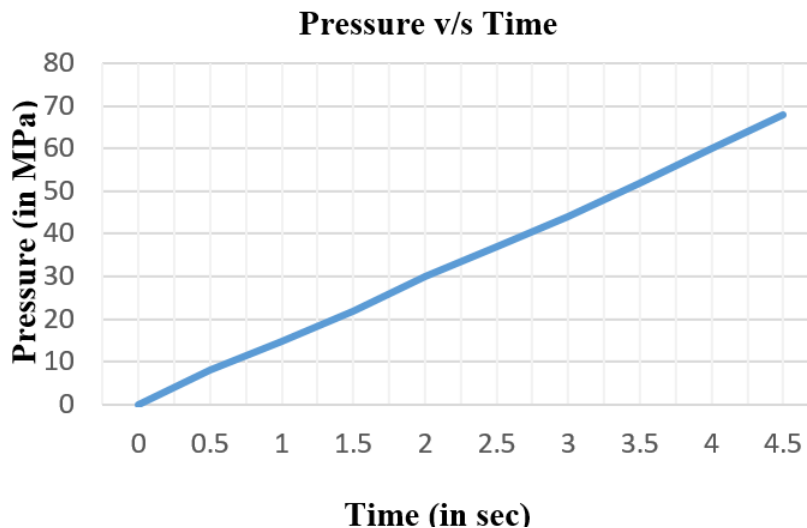


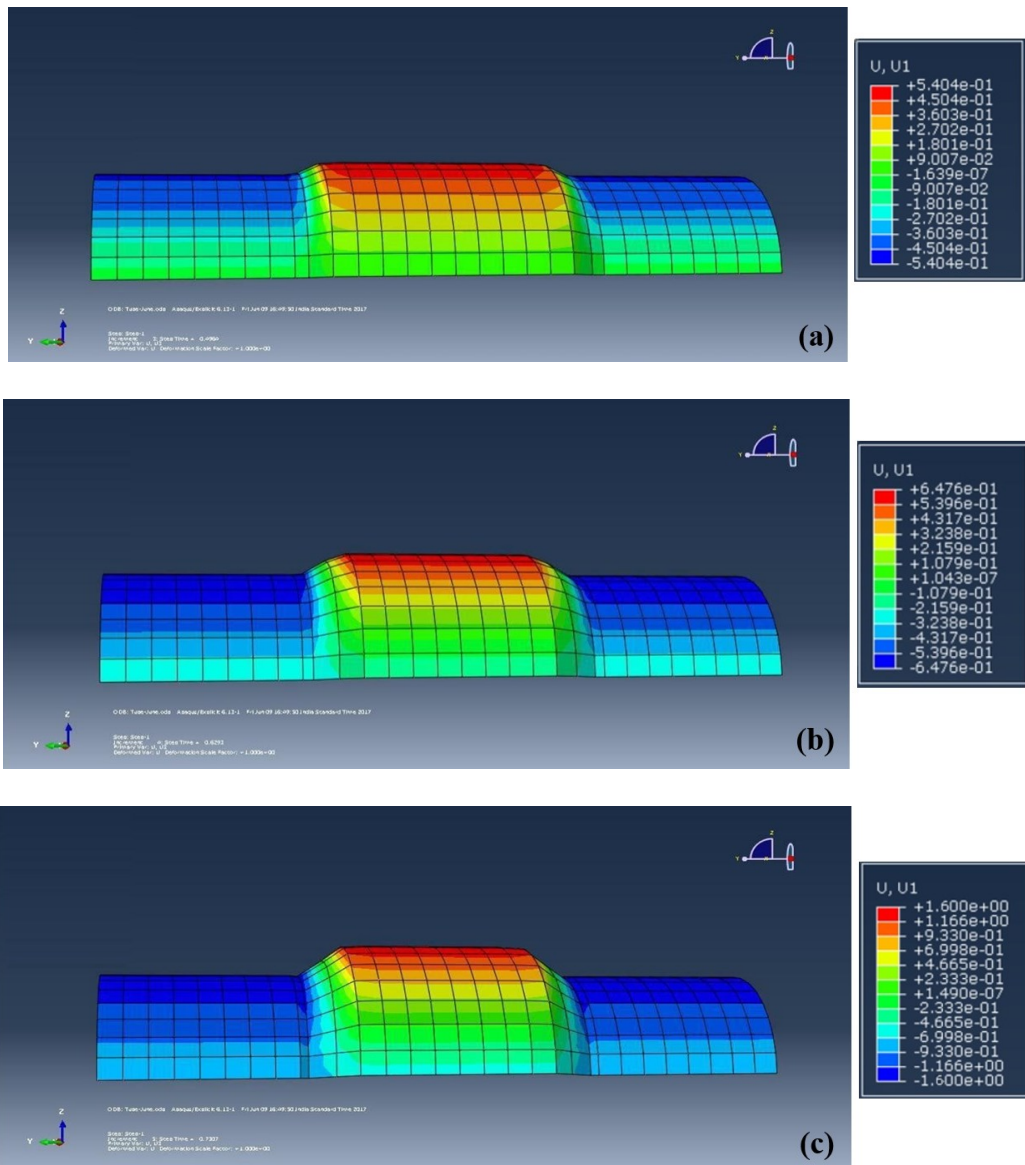
Figure 5. The loading path of the sample was taken in the simulation.

The tube wall experiences both stretching as well as bending motions while hydroforming. Due to their efficiency in resolving bending problems, linear quadrilateral elements are chosen for use in such simulations. 350 nodes and 312 elements make up the modeled tube section [17]. Die, which is

made to be a stiff surface, serves as the master surface while the tube surface serves as the slave surface. The assumed friction coefficient is 0.1. The finite sliding approach is used to formulate the interaction of the tube surface with the die and allows for the separation of two surfaces during sliding. As depicted in Fig. 4, the pressure rises linearly at a rate of 2.5 MPa/s.

5.2. Experimental Analysis

The axial force of 1000 kN is applied with a stopper provided at the two ends of the die in order to stop the ram after sealing the tube samples. The internal pressure varies from 30 MPa to 70 MPa with an interval of 10 MPa. The different bulge heights at internal pressure 30, 40, 50, 60 and 70 MPa are shown in fig. 6(a)-(e). From the figure, we can clearly demonstrate that, by increasing the internal pressure, the bulge height increases.



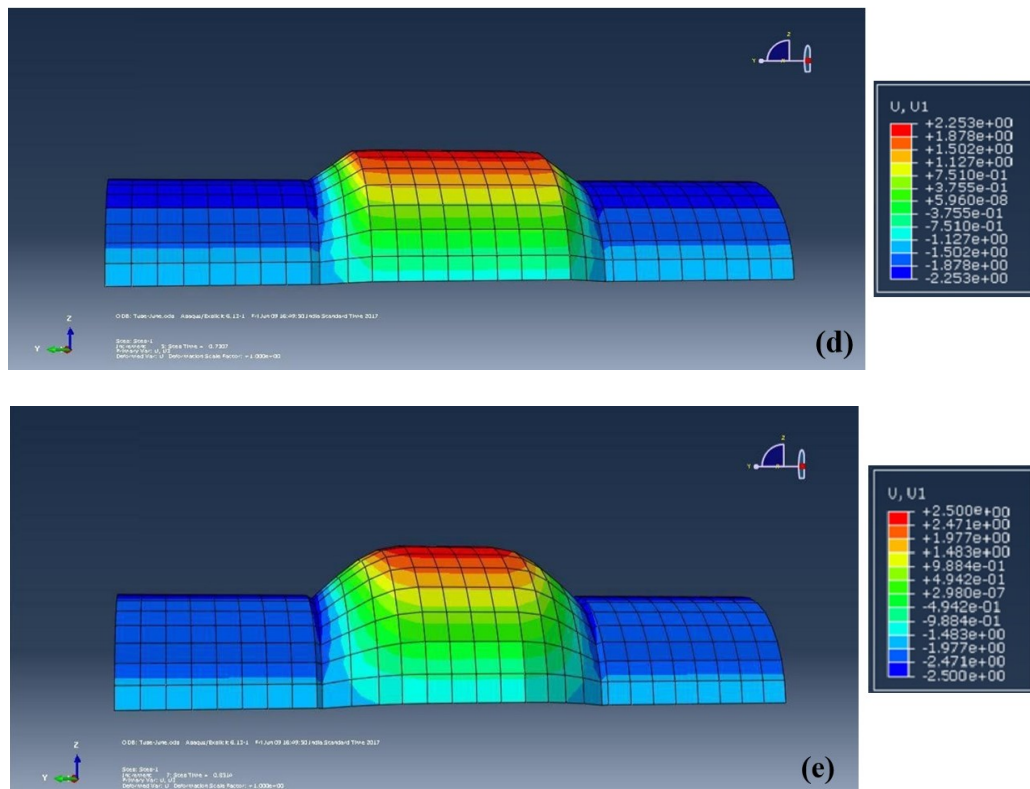


Figure 6(a) to (e). Bulge height simulation results at internal pressure of 30MPa, 40MPa, 50MPa, 60MPa and 70 MPa respectively

5.3. Measurement of bulge height and corner radius of the hydroformed tube

The initial dimensions of the tube sample consist of an outer diameter of 12.7 mm, length of 175 mm, and thickness of 0.5 mm. During the experiment, the upper and lower dies were used to lock each other with the help of a clamping pin.

5.3.1. Measurement of bulge Height at different internal Pressures

The formed parts at different internal pressures such as 30, 40, 50, 60 and 70 MPa are shown in fig. 7 (a-e). For internal pressure of 30 MPa, the obtained bulge height is 0.5 mm from the outer surface of the sample. The bulge height increases as internal pressure increases and is measured at internal pressures of 40,50,60 and 70 MPa as 1.25 mm, 1.85 mm, 2.25 mm and 2.5 mm respectively. The reason behind the increase in bulge height is the contact area between the die cavity and tube sample, as internal pressure increases, bulge height increases.

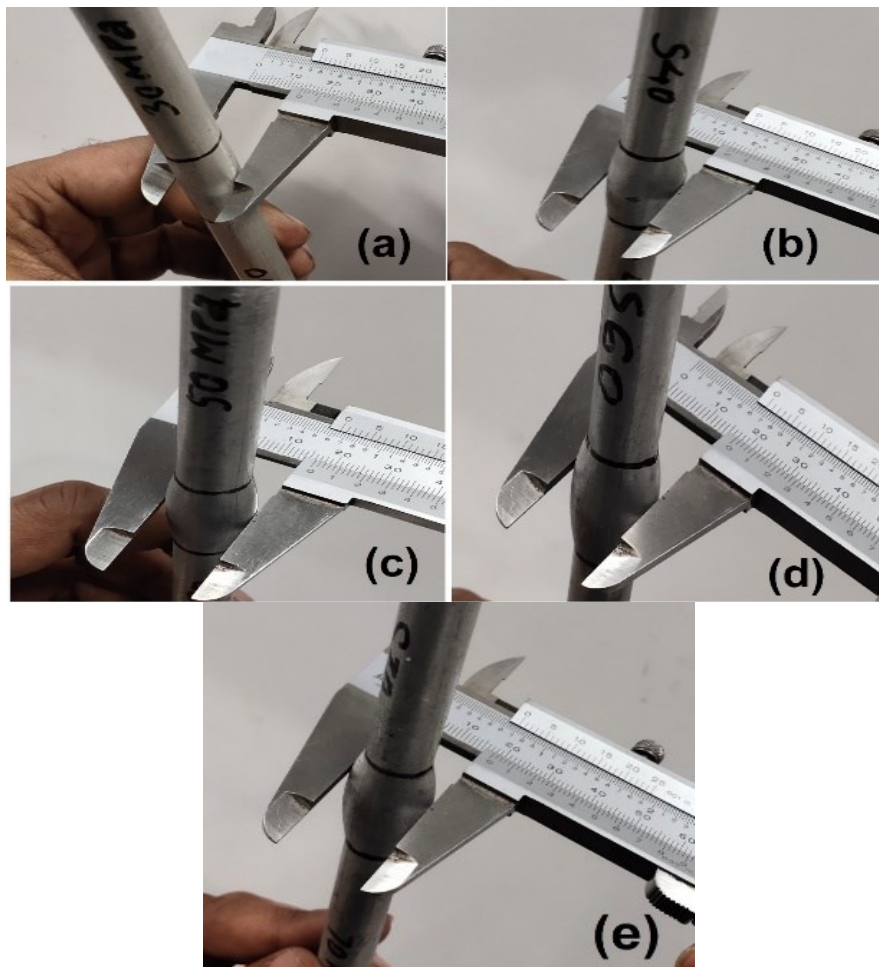


Figure 7(a) to (e). Measurement of bulge height of tube samples formed at internal pressures of 30 MPa, 40 MPa, 50 MPa, 60 MPa and 70 MPa respectively

5.3.2. Measurement of corner radius at different internal pressures

The sample corner radius (r_s) is measured and compared with the die corner radius (r_d) at different internal pressure as shown in fig. 8 (a-e). The section of the forming tube samples at different pressures was taken out and their corner radius was calculated. The sample corner radius was found more as compared with the die corner radius. For an internal pressure of 30 MPa, the sample corner radius was calculated as 11.1 mm.

At 40, 50, 60 and 70 MPa internal pressures, the sample corner radius was calculated as 10.6 mm, 9.2 mm, 8.5 mm and 5 mm respectively. The sample corner radius decreases with the increase in internal pressure because the curved formation of the tube increases.

The Variation in the bulge height and corner radius of the samples for different internal pressures is plotted. The bulge height and corner radius enforce a vital role in defining the quality of hydroforming. Here half portion of the symmetrical elliptical cross-section was chosen to study the distribution of bulge height and corner radius.

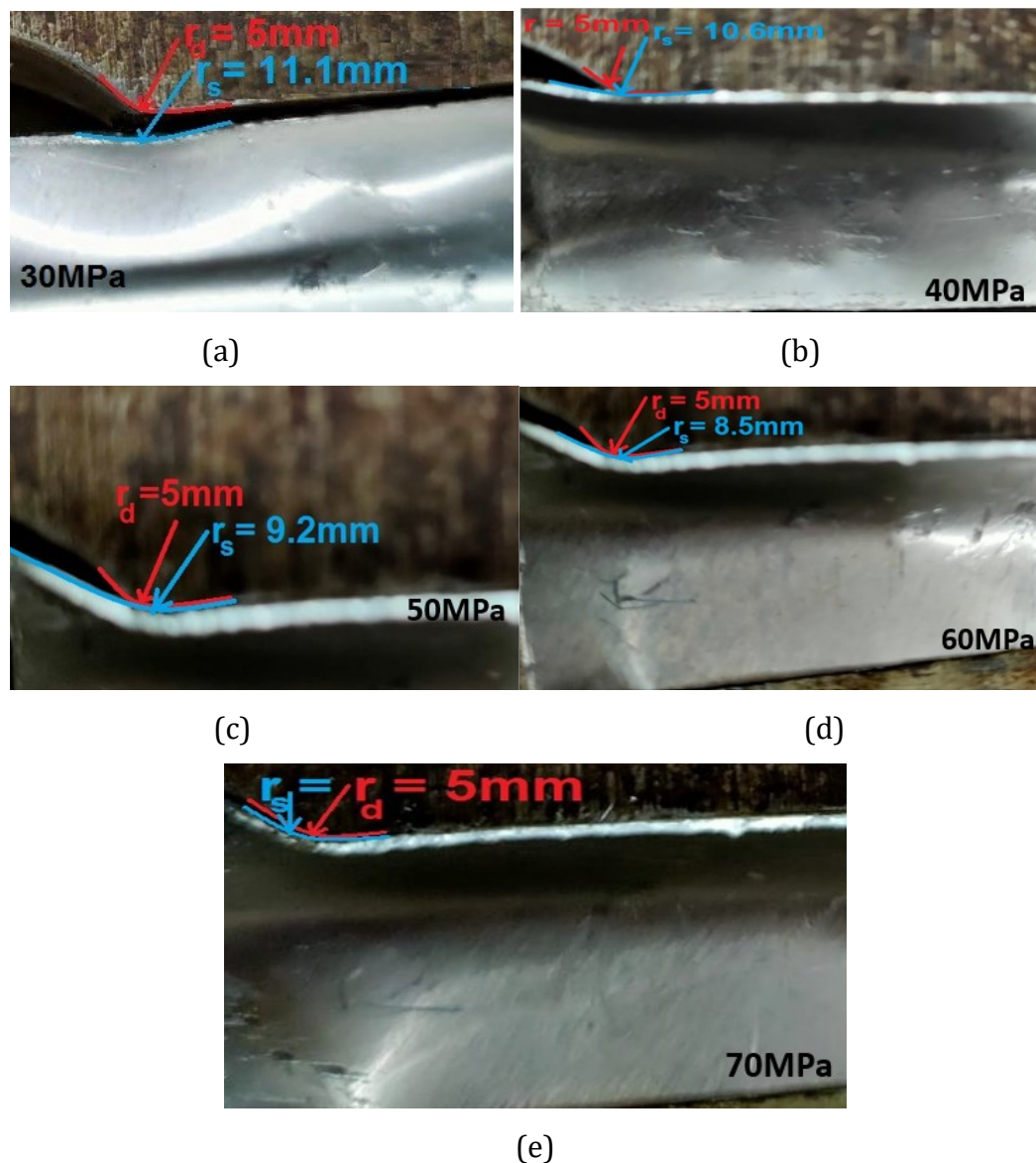


Figure 8(a) to (e). Measurement of bulge height of tube samples formed at internal pressures of 30 MPa, 40 MPa, 50 MPa, 60 MPa and 70 MPa respectively

5.3.3. Comparison of experimental results with simulation results

The experiment is carried out at different internal pressures such as 30, 40, 50, 60 and 70 MPa and simultaneously bulge height is measured. The axial force of 1000 KN is used to seal the tubes from two ends and is kept constant during the hydroforming process. To study the bulge height at different internal pressures of the hydroforming parts, we selected the internal pressures of 30, 40, 50, 60, and 70 MPa. Simultaneously simulation is carried out to plot the deviation between experimental and simulation results. The simulative loading time, t is 5s, and the coefficient of friction is taken as $\mu=0.1$. The effect of variation in bulge height due to change in

internal pressures at the end of the expansion process of the tube in an elliptical die and the percentage error between simulated and experimental data are shown in fig.9 (a) and (b) respectively. Bulge height is significantly increased with an increase in internal pressures and reached up to 2.5 mm at 70 MPa as the major elliptical height of the die is constrained to 2.5 mm. The difference in bulge height for simulation and experimentation gradually increases. Experimentally low bulge height was achieved at different internal pressure ranges until it reached the final bulge height as compared to simulative bulge height.

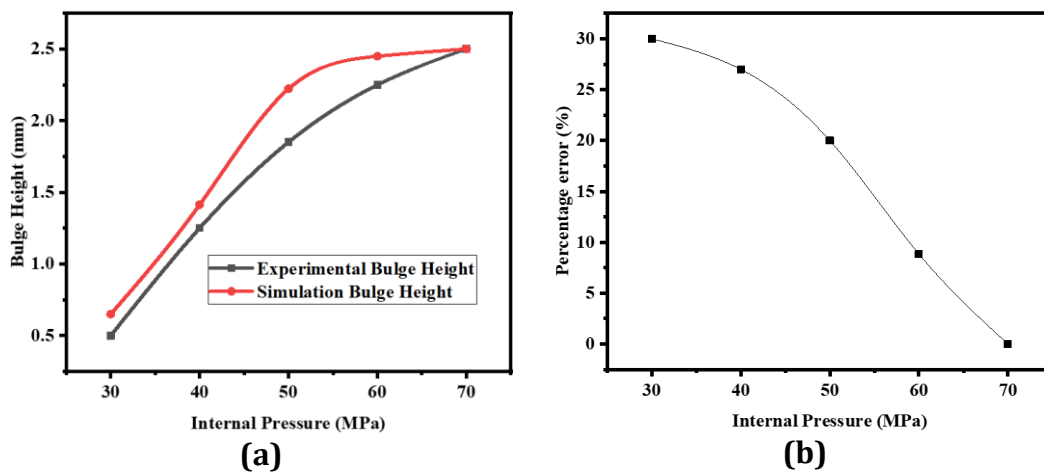


Figure 9(a). Bulge height v/s internal pressure **(b).** The percentage error in bulge height with internal pressure.

This may be due to various other parameters such as loading path, strain hardening coefficient and variation in friction coefficient between experimental and simulation. Strain hardening coefficient has a high influence on the formability of the tube so that for forming of materials with a higher value of n , Lower internal pressure is needed, but the change in thickness in such materials is higher than in others resulting in lowering of strain hardening coefficient and the friction between die walls and tube increase.[14]

5.3.4. Effects of internal pressures on bulge height

The simple percentage error between simulation and experimental bulge height results in data obtained for different pressure ranges. The formulae used to obtain percentage error are as follows:

$$\text{Percentage error} = \frac{EBH - SBH}{EBH} \times 100 \quad (1)$$

Where,

EBH = Experimental bulge height, SBH = Simulation bulge height

The percentage error in simulation data with the experimental data for bulge height is gradually decreasing (as shown in fig. 9 (b)). It bulges under the constrained condition of the die cavity. Experimental frictional resistance is large as compared to the resistance offered in the ideal condition of simulation. The targeted maximum bulge height is achieved prior to simulation than in an experiment. Simulation results show, that at around 62MPa internal pressure bulge height was achieved approximately. But experimentally, more pressure is required as it is assumed through simulation. The reason behind bulge height increases is due to an increase in material flow rate and also an increase in frictional resistance offered by the die wall due to a gradual increase in flow rate. More bulging means more outer surface comes in contact with the die wall, the die wall offers resistance to the flow tube outer surface which decreases the material flow rate.

5.3.5. Effects of internal pressures on corner radius

When materials start filling in the die cavity with the application of internal pressure, its circular cross section at the bulge portion varies and the outer surface bends at the corner chamfer of the die cavity. As internal pressure increases, the tube outer surface at the die chamfer folds gradually and the sample outer profile makes a radial curve with the die gradually decreasing. The increase in internal pressure reduces the corner radius as shown in fig.8 (a) to (e). The graph of corner radius reduction with rising internal pressures is plotted in Fig. 10 (a). The graph between simulative and experimentation percentage error with rising of internal pressures is plotted in Fig. 10 (b).

The percentage error for corner radius between simulated and experimental data increases first up to 60 MPa then decreases. The percentage error is measured according to the formulae,

$$\text{Percentage error} = \frac{ECR - SCR}{ECR} \times 100 \quad (2)$$

Where,

ECR = Experimental corner radius, SCR = Simulation corner radius

Simulative Corner radius reduces ideal frictional coefficient conditions between contacts of tube outer surface and dies inner chamfer cavity. The simulative friction coefficient is considered as 0.1 whereas experimentally it offers large frictional resistance and low strain hardening coefficient due to rapid reduction in thickness due to this, it has more corner radius than corner radius measured during simulation. Since the maximum targeted corner radius is conforming the shape of the die corner radius of 5mm, Simulation and experimental final sample corner radius after complete filling of materials were found to be equal in magnitude.

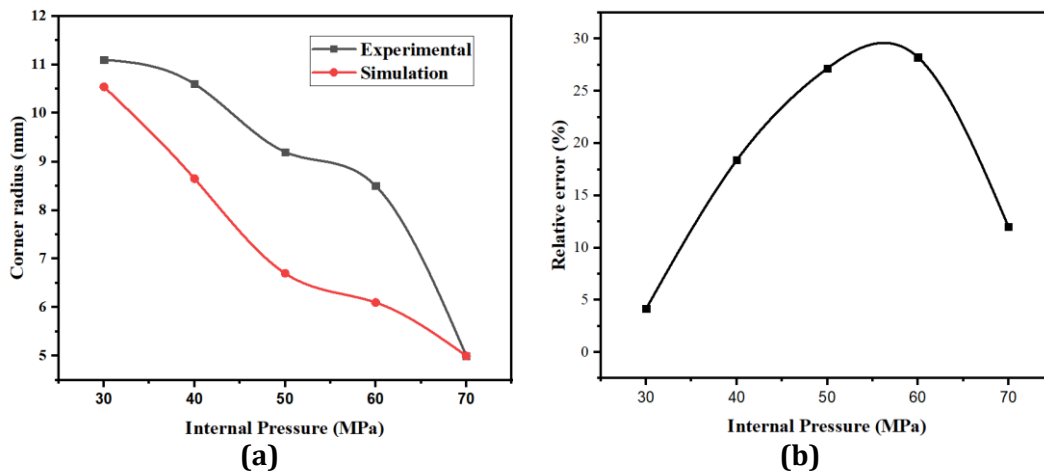


Figure 10(a). Corner radius variation with internal pressure **(b).** The percentage error in corner radius with internal pressure.

6. CONCLUSION

A Series of experiments, testing and trials were carried out on die and tooling to develop an experimental tube hydroforming machine set-up. The experiments were performed and measured different bulge heights and corner radius formed in an elliptical tube subjected to various internal pressures and again validated with numerical simulation. It was observed that simulated and experimental data are comparatively matched with each other with a slight deviation. The simulated results show high bulge height achieved early subjected to a defined internal pressure as compared with experimentally obtained bulge height for the same pressure range. The bulge height increases as internal pressure increases and experimentally measured at internal pressures of 30, 40, 50, 60 and 70 MPa as 0.5 mm, 1.25 mm, 1.85 mm, 2.25 mm and 2.5 mm respectively. The simulation results on bulge height are 0.54 mm, 0.65 mm, 1.6 mm, 2.25 mm and 2.5 mm at an internal pressure of 30, 40, 50, 60 and 70 MPa respectively.

The maximum bulge height is achieved by conforming to the shape of the maximum undercut cavity provided inside the die of 2.5 mm which is similar for both simulation and experimental. The bulge height of 2.5 mm was achieved through simulation at an internal pressure of approximately 62 MPa whereas experimentally it takes 70 MPa.

The corner radius obtained during the experiment is also compared with simulation and it is found that the corner radius obtained through simulation is less than the experimentally obtained results. This is because of ideal friction coefficient taken during simulation is 0.1 and but in reality, the friction coefficient during the experiment is not ideal as we assume during simulation. From experimental investigation, it is observed that the frictional resistance at the contact of tube outer surface and die wall cavity corner radius plays a significant role to get optimum quality of the components or products. Strain hardening is also an important parameter to define material

flowability. Strain hardening coefficient has a high influence on the formability of the tube so that for forming of materials with a higher value of n , Lower internal pressure is needed, but a change in thickness in such materials is higher than in others resulting in lowering of strain hardening coefficient and the friction between die walls and tube increase. The impact of internal pressure on tube hydroforming quality was inspected. During the hydroforming process, the corner radius reduces, and bulge height increases continuously during the rising of internal pressure. Experimentally, the tube sample was completely filled in the die cavity at a pressure of 70 MPa.

ACKNOWLEDGEMENTS

The authors wish to express their deepest gratitude to BRNS for funding the project GP/LT/ME13-14/03 titled "Technology development & fabrication of table-top CNC machine for micro tubular-hydroforming with process optimization".

REFERENCES

- [1] Hirsch J and Al-Samman T, **Superior light metals by engineering: optimized aluminum and magnesium alloys for automotive applications**, *Acta Mater* 2013; 61:818–843.
- [2] Han S, Woo Y, Hwang T, Oh I, Hoon Y. Moon, **Tailor layered tube hydroforming for fabricating tubular parts with dissimilar thickness**, *Int J Mach Tools Manuf* 2019; 138:51–65.
- [3] Bell C, Corney J, Zuelli N, Savings D, **A state of the art review of hydroforming technology: its applications, research areas, history, and future in manufacturing**, *Int J Mater Form* 2019; (1–3).
- [4] Lee MG, Korkolis YP, Kim JH, **Recent developments in hydroforming technology**, *J Mater Process Technol* 2015; 229(2):572–596.
- [5] Bapurao G. Marlapalle & Rahulkumar S. Hingole, **Predictions of formability parameters in tube hydroforming process**. *SN Applied Science* 2021; 606:1109.
- [6] Abbassi F, Ahmad F, Gulzar S, Belhadj T, Karrech A, Choi H, **Design of T-shaped tube hydroforming using finite element and artificial neural network modeling**, *J Mech Sci Technol* 2020; 34(3):1129–1138.
- [7] Hashemi R, Bostan Shirin M, Einolghozati M, et al, **A different approach to estimate the process parameters in tube hydroforming**, *Int J Mater Form* 2015; 8: 355–366.
- [8] Kim CI, Yang SH and Kim YS, **Analysis of forming limit in tube hydroforming**, *J Mech Sci Tech* 2013; 27: 3817–3823.
- [9] Ngaile G, Lowrie J, **Punch design for floating based micro-tube hydroforming die assembly**, *J Mater Proc Technol (2018)* 253: 168–177.
- [10] Xiangwen Fan, Jianwei Liu, Xinqi Yao, Jiahao Feng, **Investigation of Formability of Metal Thin-Walled Tubes Based on the Tube Hydroforming**, *AIAM 2019: Proceedings of the 2019 International*

- Conference on Artificial Intelligence and Advanced Manufacturing* (2019) 25:1-4.
- [11] C. Han, Q. Liu, H. Lu, G. L. Gao, W. C. Xie & S. J. Yuan, **Thickness improvement in hydroforming of a variable diameter tubular component by using wrinkles and preforms**, *The International Journal of Advanced Manufacturing Technology* (2018) 99:2993-3003.
- [12] Yuan SJ, Cui XL and Wang XS, **Investigation into wrinkling behavior of thin-walled 5A02 aluminum alloy tubes under internal and external pressure**, *Int J Mech Sci* (2015) 92: 245–258.
- [13] Yuan, S, **Stress-Strain Analysis for Tube Hydroforming**. In: **Modern Hydroforming Technology**, Springer eBook, Singapore (2020) 155-169.
- [14] **Principles of Metal Manufacturing Processes, Chapter 3 Stress and strain during deformation** "[https://books.google.com/books/about/Principles_of_Metal_Manufacturing_Proces.html?id=hZsNZTDU1G0C.](https://books.google.com/books/about/Principles_of_Metal_Manufacturing_Proces.html?id=hZsNZTDU1G0C)"
- [15] AMTS 2022 | *Shanghai International Automotive Manufacturing Technology & Material Show* (shanghaiamts.com)
- [16] Cui XL, Wang XS, Yuan SJ, **Further assessment of the plastic instability of thin-walled tubes in double-sided hydro-bulging process with verification experiments**, *Proc IMechE, Part B: J Engineering Manufacture* (2018) 233: 776–786.
- [17] ABAQUS/Standard, User Manual, Version 5.8.
- [18] Zicheng Zhanga, Yajun Kanga, Tsuyoshi Furushimab, Ken-ichi Manabec, Cong Wangd, Bin Lia, **Deformation behavior of metal micro tube during hydroforming process**, *18th International Conference Metal Forming 2020*. 50(2020) 328-331.
- [19] Hajime Yasui, Taisuke Miyagawa, Shoichiro Yoshihara, Tsuyoshi Furushima, Ryuichi Yamada and Yasumi Ito, **Influence of Internal Pressure and Axial Compressive Displacement on the Formability of Small-Diameter ZM21 Magnesium Alloy Tubes in Warm Tube Hydroforming**, *Metals* (2020) 674-690.
- [20] Yeong-Maw Hwang, Hong-Nhan Pham and Hiu-Shan Rachel Tsui, **Investigation of Punch Shape and Loading Path Design in Hydro-Flanging Processes of Aluminum Alloy Tubes**, *Metals* (2020) 636-353.
- [21] Han S, Woo Y, Hwang T, Oh I, Hoon Y Moon, **Tailor layered tube hydroforming for fabricating tubular parts with dissimilar thickness**, *Int J Mach Tools Manuf* (2019)138:51–65.
- [22] Kong TF, Lu XZ, Chan LC, **Analysis and reduction of wrinkling defects for tube-hydroforming magnesium alloy components at elevated temperatures**, *Mater Des* (2019)173:107761.
- [23] Reddy PV, Reddy BV, Ramulu PJ, **An investigation on tube hydroforming process considering the effect of frictional coefficient and corner radius**, *Adv Mater Process Technol* (2020) 6(1).

- [24] Colpani A, Fiorentino A, Ceretti E, **Characterization and optimization of the hydroforming process of AISI 316L steel hydraulic tubes**, *Int J Adv Manuf Technology* (2020)107(1-2):293-309.
- [25] Zhu H, He Z, Lin Y, Zheng K, Fanb X, Yuan S, **The development of a novel forming limit diagram under nonlinear loading paths in tube hydroforming**, *Int J Mech Sci* (2020) 172:105392.